Journal of Materials Chemistry C

Accepted Manuscript

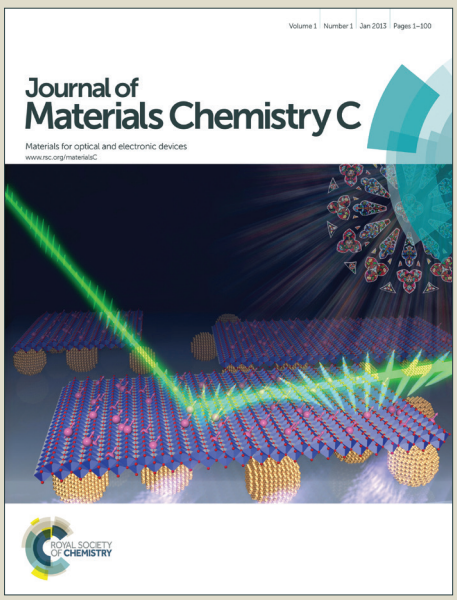

ROYAL SOCIETY OF CHEMISTRY

www.rsc.org/materialsC

Journal Name

RSCPublishing

ARTICLE

Solid-state electrochemical reduction process of magnetite in Li batteries: in-situ magnetic measurements toward electrochemical magnets†

Cite this: DOI: 10.1039/xoxxoooooox

Received ooth January 2012,
Accepted ooth January 2012

DOI: 10.1039/xoxxoooooox

www.rsc.org/

Tetsuya Yamada,[a,b] Kantaro Morita,[a] Keita Kume,[a] Hirofumi Yoshikawa*,[a] and Kunio Awaga*,[a,b]

The solid-state electrochemical reduction of magnetite (Fe_3O_4) nanoparticles was studied using a miniature Li battery that included Fe_3O_4 as a cathode active material. X-ray diffraction and absorption analyses clearly elucidated the relation between the battery voltage and the chemical species reduced from Fe_3O_4. Upon discharging, the Fe_3O_4 nanoparticles suffer a 1.4-electron reduction in the voltage range from 2.9 to 1.3 V, while maintaining the original inverse spinel structure. This process is reversible, so that the Li-Fe_3O_4 battery can be rechargeable with a fairly large capacity of 160 A h kg^{-1}. In the range below 1.3 V, Fe_3O_4 is irreversibly reduced to α-Fe through $Li_xFe_3O_4$, with drastic changes in structure. This electrochemical process exhibits nanomilling for α-Fe. In-situ magnetic measurements supported this two-step conversion, and indicated a ferrimagnetic ordering of $Li_xFe_3O_4$ at T_N = *ca.* 150 K and superparamagnetic behavior of α-Fe. Furthermore, the reversible solid-state electrochemical reaction in the range between 1.8 and 1.3 V was associated with a controllable change in magnetization (13%), suggesting this reaction might be applied to the development of "electrochemical magnets."

Introduction

Solid-state electrochemistry (SSE) is a comprehensive discipline which covers various topics from fundamental sciences to practical applications.[1-3] In conventional SSE, the potential difference between the working and counter electrodes induces redox reactions of the electrode active materials on the working electrode. Research and development of rechargeable batteries is one of the most important areas in SSE. Recently, we developed a molecular cluster battery in which the anode was a Li metal and the cathode consisted of a transition-metal cluster complex such as $Mn12$[4-7] or polyoxometalate (POM).[8-10] These new batteries have high capacities, due to the formation of the super-reduced chemical species of the molecular clusters, namely $[Mn12]^{8-}$ and $[POM]^{27-}$. It is notable that the redox states of these materials can be controlled by the electrochemical potential of the cathode in SSE. Indeed, SSE can provide an excellent method for the production of new materials and for precise control of the valence states of the redox-active materials. The latter automatically brings about controlled physical properties, such as conductivity and magnetism. To elucidate this advantage of SSE, we have developed an in-situ magnetic measurement system under SSE, including a miniature lithium-battery cell (see Fig. S1) that can be inserted into a conventional SQUID susceptometer. By adopting a redox-active target compound as cathode, we can perform operando magnetic measurements during its solid-state redox reactions at room temperature. In addition, while keeping the redox potential constant, variable-temperature magnetic measurements are available down to 2 K. We have already applied this system to a mixed-valent chromium Prussian-blue ferrimagnet, $Cr_{2.24}[Cr(CN)_6]\cdot Cl_{0.13}(OH)_{1.68}\cdot 5.25H_2O$ (Cr-PBA),[11] with a ferrimagnetic transition temperature T_N of 215 K, and found continuous changes in T_N and the saturation magnetization, which were well understood by the redox/spin changes of the Cr ions, though these magnetic changes occurred at low temperatures.

To achieve high-temperature magnetic control under SSE, metal oxides are promising materials because of their high transition temperatures and redox activities. Magnetite, Fe_3O_4 ($Fe^{III}[Fe^{II}Fe^{III}]O_4$), is the oldest magnet known to be used by humans. Its structure is composed of Fe^{III} ions located at a tetrahedral site (A site), and mixed valent Fe^{II} and Fe^{III} ions located in equal amounts at the octahedral site (B site) in the inverse spinel structure (see Fig. 1(a)), and it exhibits a ferrimagnetic ordering at T_N=850 K.[12] Since its discovery as loadstone in the 6th century B.C., this magnet has been utilized in various tools and instruments, such as compasses, magnetic fluids, contrast agents for magnetic resonance imaging and vehicles for drug delivery.[13-15] In addition to its practically applicable magnetism, magnetite has attracted academic

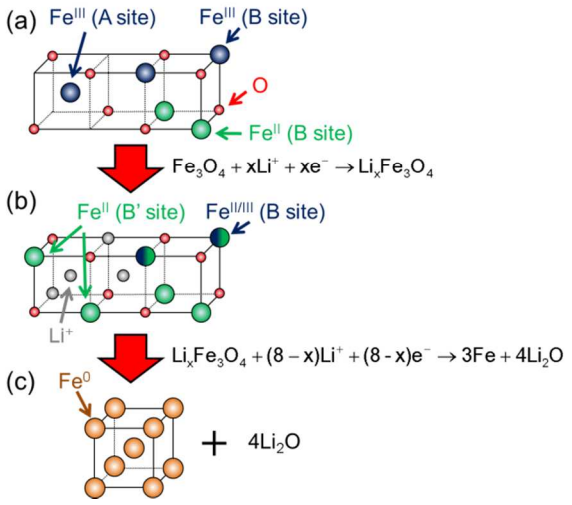

Fig. 1 Structural changes in the electrochemical reduction process of Fe_3O_4: (a) the inverse spinel structure for Fe_3O_4, (b) the rocksalt structure for $Li_xFe_3O_4$, and (c) the body-centered cubic structure for α-Fe. In the panels (a) and (b), the B site is randomly occupied by Fe^{II} or Fe^{III} ions.

interest due to its Verwey transition, half-metallic behavior, and superparamagnetism of nanoparticles.[16-18] In addition, this compound is known to operate as an electrode active material of lithium batteries with a significantly large discharge capacity of over 1500 Ah/kg in the voltage range from *ca.* 3 to 0 V. This voltage-change process was explained by the electrochemical reduction from the inverse-spinel Fe_3O_4 to Fe metal[19-21] through the rocksalt phase of $Li_xFe_3O_4$,[21-23] though the precise relation between the battery voltage and the chemical state of Fe, and the reversibility of this redox process, were not elucidated. Further, the ex-situ magnetic measurements before and after the reduction from Fe_3O_4 to $Li_xFe_3O_4$ indicated a decrease in the saturation magnetization at room temperature, and gave a rough estimation of T_N as *ca.* 150 K for $Li_xFe_3O_4$.[21]

In the present work, we performed in-situ magnetic measurements and ex-situ X-ray structural analysis for the whole electrochemical process from Fe_3O_4 to Fe metal, in order to achieve a comprehensive understanding of this solid-state redox process, which would explain the large battery capacity of magnetite, and provide a controllable magnetism by SSE. By making a Li-Fe_3O_4 battery, which was composed of lithium metal as the anode and magnetite nanoparticles as a cathode active material, we examined the relationship between the electrochemical reactions and magnetic properties, and the switchable magnetic change of Fe_3O_4 at room temperature by the electrochemical potential control. Based on the results of these examinations, we designed an "electrochemical magnet," which we describe herein.

Experimental

Fe_3O_4 nanoparticles with an average diameter of 30 nm were purchased from Sigma-Aldrich. A Li battery cell was constructed to perform electrochemically controlled reduction of Fe_3O_4. The cathode was prepared as follows: Fe_3O_4 nanoparticles (10 wt%) and conductive carbon black (70 wt%) were mixed with polyvinylidene difluoride (20 wt%) as a binder, and then the mixture was spread onto an aluminum plate and dried. Then, this cathode, a Li metal anode, a separator (Whatman no. 1820-125), and a 1 M $LiPF_6$ electrolyte in a mixed solution of diethyl carbonate (DEC) and ethylene carbonate (EC) (DEC/EC = 1:1 wt/wt%) were assembled into a small quartz cell (15×7×5 mm^3, see Fig. S1)[11] in an Ar atmosphere. The battery cells were connected to a charge/discharge device (Hokuto HJ1001-SM8A), and then the redox processes of Fe_3O_4 were investigated in the battery voltage range between 4.2 and 0 V versus Li/Li^+.

In-situ magnetic measurements were performed as follows: the Li-Fe_3O_4 battery, inserted into a SQUID susceptometer (Quantum Design MPMS XL5), was charged or discharged by loading or taking out, respectively, with a constant current density of 0.03 $mA{\cdot}cm^{-2}$ at room temperature (300 K). After reaching a specific voltage in the discharge process, the voltage was maintained for several hours, and then, we opened the circuit and investigated the temperature and magnetic-field dependence of the magnetization of the battery cell. Setting the sample temperature at 300 K again, the battery was further discharged to the next measurement voltage. The blank contribution was experimentally obtained by measuring the magnetization of the battery cell without the cathode. By subtracting the blank magnetization from the total of the battery, the magnetization of the cathode was obtained. Note that the magnetization of the blank cell was much smaller by three orders of magnitude than that of the cathode, which included the ferrimagnet, Fe_3O_4.

To characterize the electrochemically-generated species of the cathode samples at the specific voltages, we carried out ex-situ powder X-ray diffraction (PXRD) and Fe *K*-edge X-ray absorption fine structure (XAFS) analyses for the cathode materials, which had been in a coin-cell Li-Fe_3O_4 battery. After applying a constant voltage to it for a few hours, we disassembled the battery cells to remove the cathodes in an Ar atmosphere, and immediately performed the X-ray measurements in air, even without drying. Their PXRD patterns were measured with Cu *Kα* radiation on a Rigaku Multiflex using ex-situ cathodes, and their Fe *K*-edge XAFS spectra were recorded from 6800 to 8200 eV in a transmission mode using the beamline BL5S1 at Aichi Synchrotron Radiation Center, Aichi, Japan.

Results and discussion

Structural analysis of the electrochemical reduction of Fe_3O_4

The reduction process of Fe_3O_4 by Li metal was reexamined in the Li-Fe_3O_4 battery cells. This process has been reported to consist of two steps, as schematically shown in Fig. 1: (i) the reductive insertion of Li^+ ions to form $Li_xFe_3O_4$ and (ii) the generation of Fe metal.[20, 21] Figure 2(a) shows the first discharge curve of the Li–Fe_3O_4 battery from 4.2 to 0 V, in

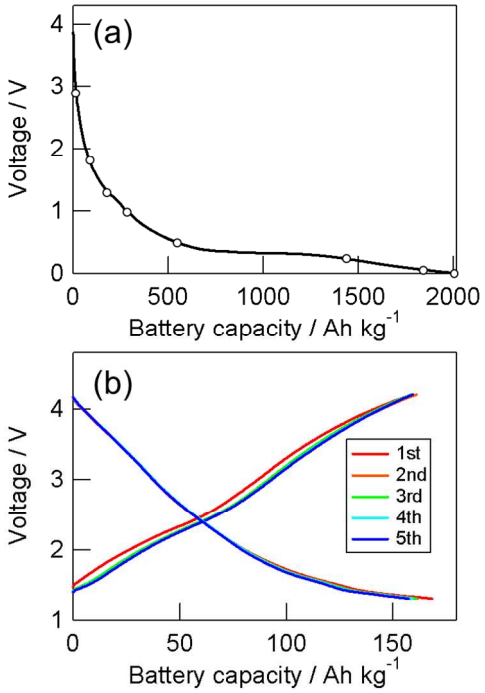

Fig. 2 (a) The first discharge curve of the Li-Fe_3O_4 battery at 300 K, in which the capacity is normalized by the weight of Fe_3O_4 in the cathode. The open circles indicate the voltages at which the in-situ magnetic measurements were carried out. (b) Charge/discharge performance for five cycles between 4.2 and 1.3 V with a load current of 0.03 mA·cm^{-2}.

which the capacity is defined per unit weight of Fe_3O_4. This curve exhibits a gradual decrease in voltage, and finally reaches a capacity of *ca*. 2000 Ah/kg at 0 V. Such behavior is consistent with that reported previously.[19] It is known that this discharge/charge process is irreversible and the discharge capacity at the second cycle or later is significantly smaller than the first one.[19] Since the theoretical capacity, caused by 1-electron reduction of Fe_3O_4, is 116 Ah/kg (see the Electronic Supplementary Information), the observed battery capacity is much larger than the theoretical one for the 8-electron reduction from Fe_3O_4 to Fe. It is considered that this excess capacity is caused by an electrochemical reduction of the electrolyte, the formation of a solid electrolyte interface (SEI),[24] and/or a capacitor effect caused by the formation of electric double layers. In the present work, however, taking the ex-situ X-ray and in-situ magnetic data into account, we found an electrochemically reversible voltage range for the Li-Fe_3O_4 battery, with a good charge/discharge cyclability. Figure 2(b) shows the charge/discharge curves for the first five cycles in the battery voltage between 4.2 and 1.3 V, indicating little decay. These capacities (*ca*. 160 A h kg^{-1}) suggest a 1.4 electron reduction from the initial state, namely Fe_3O_4. It is concluded that the Li-Fe_3O_4 battery operates as a rechargeable battery in the range above 1.3 V. Although, in the present study, the weight ratio of magnetite in the cathode is only 10%, which is too low for practical applications, the unit-weight capacity of this cheap and environmentally friendly cathode active material corresponds to those of the conventional Li-ion batteries (*ca*.

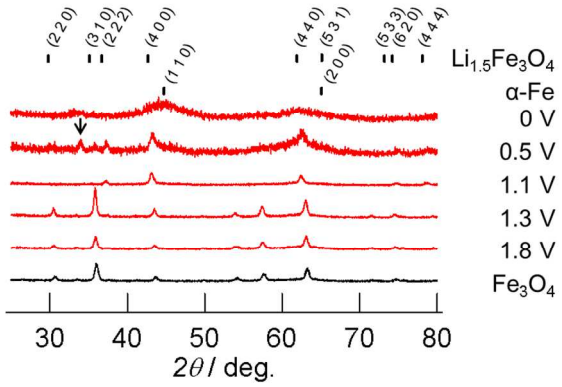

Fig. 3 Ex-situ PXRD patterns for the electrochemically reduced species of Fe_3O_4 in the Li- Fe_3O_4 battery during discharge. The vertical bars indicate the patterns of rocksalt-type $Li_{1.5}Fe_3O_4$[20] and α-Fe metal.[25] The arrow at 0.5 V indicates the XRD peak assignable to Li_2O.

150 A h kg^{-1}), which are based on expensive and toxic metals such as Co and Ni.

To understand the relation between the battery voltage and the structure of the cathode active material, ex-situ PXRD measurements were performed at 1.8, 1.3, 1.1 0.5 and 0 V. The results are shown in Fig. 3, where the diffraction patterns of the authentic Fe_3O_4, the rocksalt $Li_{1.5}Fe_3O_4$[20] and α-Fe[25] are also shown for comparison. The PXRD patterns of the cathode samples above 1.3 V are the same as that of Fe_3O_4, indicating the inverse spinel-type structure. At 1.1 V, however, the PXRD pattern changes completely, and the new pattern can be assigned to $Li_xFe_3O_4$, which crystallizes into a rocksalt-type structure with a lattice constant of 8.47 Å.[20] As shown in Fig. 1(b), this structure can be understood as the result of a site shift of the Fe ions from A to vacant B, which is denoted by B', in the inverse spinel structure and the insertion of Li^+ ions into A and the remainder of the B' sites.[20, 21] At 0 V, the PXRD pattern exhibits significantly broad peaks, which indicate the formation of α-Fe metal with a body-centered cubic (bcc) structure (see Fig. 1(c)).[26] This process should be associated with the elimination of Li_2O from the lattice. Actually, the peaks around 2Θ = 35° at 0.5 V are ascribable to those of Li_2O. When the battery was recharged from 0 to 4.2 V, we found a recovery of the rocksalt phase. This indicates that the structural change between the rocksalt phase and Fe metal is reversible, even though this is associated with the insertion/disinsertion of Li_2O.

The Fe *K*-edge X-ray absorption near edge structure (XANES) spectra of the ex-situ cathode samples were examined in the voltage range from 2.6 to 0 V. The results are shown in Fig. 4, in comparison with those of the standard samples, $Fe^{II,III}{}_3O_4$, $Fe^{II}O$ and Fe^0 foil. In the voltage range from 2.6 to 1.4 V, the absorption edge of the cathode sample exhibits a small low-energy shift, followed by a significant low-energy shift of the absorption peak at 1.0 V. The spectrum at 1.0 V fairly resembles that of $Fe^{II}O$. At 0.1 V, the signal shape is nearly identical to that of Fe^0, through a change at 0.7 V. The electrochemical reduction process of Fe_3O_4 can be explained as follows: the Fe^{III} in Fe_3O_4 is reduced to Fe^{II} while maintaining

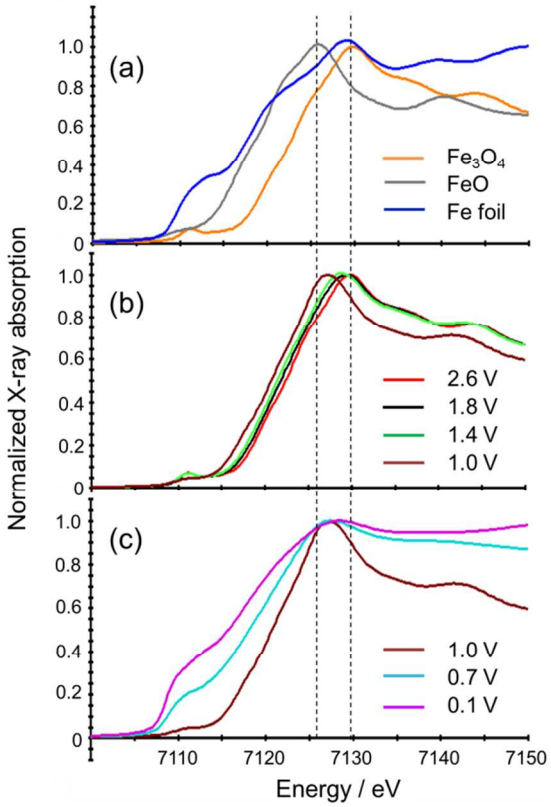

Fig. 4 Ex-situ Fe K-edge XANES spectra: (a) the standard samples, Fe_3O_4, FeO and Fe foil, (b) the electrochemically-generated species of Fe_3O_4 in the range of 2.6 and 1.0 V, and (c) those in the range of 1.0 and 0.1 V. Vertical dashed lines, indicating edge energies with a maximum X-ray absorption in XANES spectrum of Fe_3O_4 and FeO, are only guides for eyes.

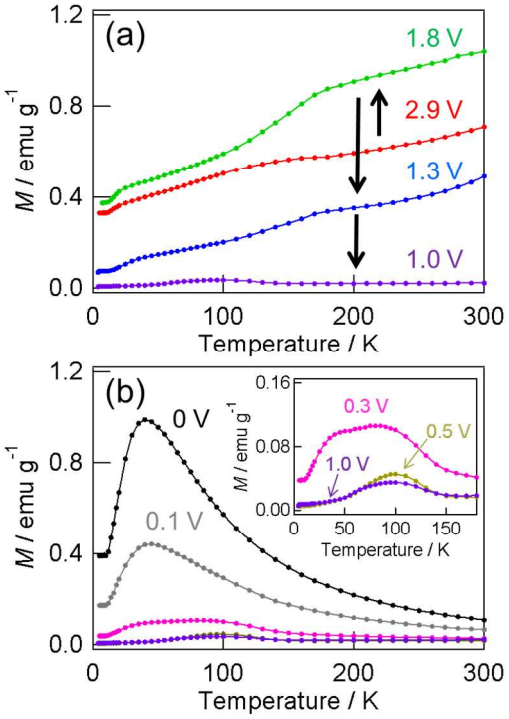

Fig. 5 Temperature dependences of the magnetizations under 100 Oe for the cathodes of the Li-Fe_3O_4 batteries in the voltage ranges from 2.9 to 1.0 V (a) and from 1.0 to 0 V (b). The inset of panel (b) shows the low-temperature behavior on an enlarged scale.

the inverse spinel-type structure of Fe_3O_4 from the initial battery voltage at 1.3 V. Note that this voltage corresponds to −1.7 V vs. the standard hydrogen electrode (SHE). Then, in the range from 1.3 to 1.0 V a drastic structural transformation to a rocksalt-type structure takes place, forming $Li_xFe_3O_4$[20] (see Fig.1(b)) after a reduction of more than 1.4 electrons. This rocksalt phase is maintained above 0.5 V, and α-Fe metal is finally formed at 0 V by a more than 6-electron reduction (see Fig.1(c)). These reduction voltages are dependent on the particle size and chemical environments of Fe_3O_4,[27, 28] since the threshold voltages for the structural changes to the rocksalt phase and to α-Fe metal, may be calculated by the numbers of reduction electrons. Note that the peak widths of the PXRD patterns at 1.8, 1.0 and 0 V indicate that the particle sizes are 26 nm for Fe_3O_4, 23 nm for rocksalt-type $Li_xFe_3O_4$, and 5 nm for α-Fe, respectively, which were calculated from a half line width of their diffraction peaks using the Scherrer equation.[29]

In-situ magnetic measurements for the reduction process of Fe_3O_4

In-situ magnetic measurements were performed to reveal the reduction process of Fe_3O_4 seamlessly from a magnetic point of view, while discharging the Li-Fe_3O_4 battery from 2.9 to 0 V. The voltages at which the magnetic measurements were performed are indicated by the open circles in Fig. 2(a); while holding each voltage, the temperature dependence of the magnetization of the whole battery cell was measured in the field of 100 Oe, upon heating from 4 K after zero-field cooling. Then, after subtracting the diamagnetic contributions from the materials except the cathode, the magnetization per unit weight of the cathode was obtained, though no compensation was made for the contributions of the other cathode components, except magnetite. The results at the voltages of 2.9, 1.8, 1.3 and 1.0 V are shown in Fig. 5(a). The magnetic properties of the as-purchased Fe_3O_4 nanoparticles are shown in Fig. S2 for comparison. The magnetizations at 2.9 V, which are considered to be caused by Fe_3O_4 before the electrochemical reduction, exhibit a gradual increase upon heating in the whole temperature range and the Verwey phase transition[16] was not observed due to a nanosize effect.[30] This temperature dependence is similar to that of authentic Fe_3O_4, while the values of the magnetizations are 10 times smaller than those of magnetizations in the whole temperature range, because the content of Fe_3O_4 in the cathode is 10 wt%. At 1.8 V, the temperature dependence of the magnetization is similar to that at 2.9 V below 100 K, but the magnetization exhibits a significant increase above this temperature. However, the magnetizations at 1.3 V become much smaller than those at 2.9 and 1.8 V. Note that this dependence on the battery voltage above 1.3 V was found to be reversible, as well as the charge/discharge curves. At 1.0 V, the magnetizations are

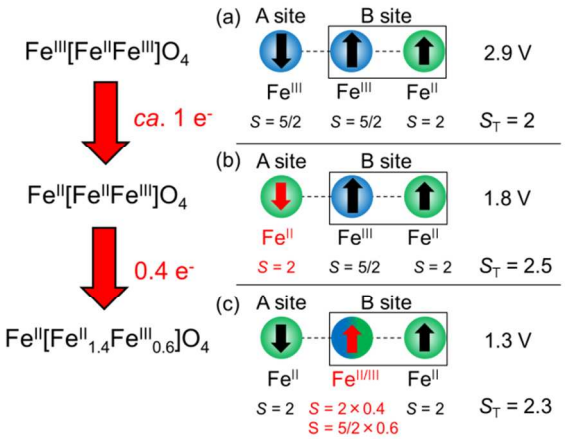

Fig. 6 Expected spin states in the reduction process of Fe_3O_4 at 2.9 V (a), 1.8 V (b), and 1.3 V (c).

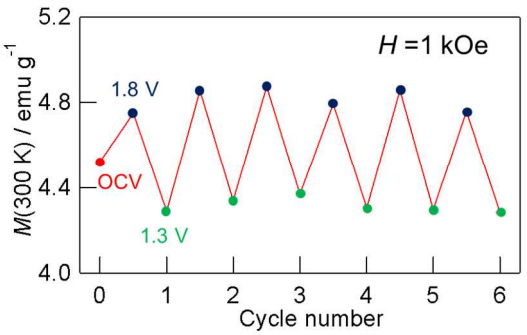

Fig. 7 Magnetization changes of the cathode of a Li-Fe_3O_4 battery during charge/discharge at room temperature, under 1 kOe. The red, blue and green circles indicate the magnetizations at the open circuit voltage (OCV, *ca.* 3.3 V), 1.8 V, and 1.3 V.

nearly collapsed throughout the whole temperature range.

The expected spin states in the reduction process of Fe_3O_4 at 2.9, 1.8 and 1.3 V are schematically shown in Fig. 6. The battery discharge capacity in Fig. 2(a) indicates that the numbers of reduction electron per Fe_3O_4 are *ca.* 0, 1, and 1.4, respectively, at these voltages. In the ferrimagnetic phase of Fe_3O_4, the spins at the A and B sites are aligned in an antiparallel fashion. Since the Fe^{III} ions at the tetrahedral A sites in the inverse spinel structure are more easily reduced than those at the octahedral B sites,[31] the total spin number, S_T, should increase from 2 to 2.5 by the 1-electron reduction of the Fe^{III} ion at the A site (see Fig. 6(b)). This increase probably causes the increase in magnetization at 1.8 V. A successive reduction is expected to occur for the Fe^{III} ion at the B site, reducing the value of S_T to 2.3 (see Fig. 6(c)). This probably corresponds to the spin structure at 1.3 V, though the magnetizations at 1.3 V are smaller than those at 2.9 V. This quantitative discrepancy could be caused by some changes in *g*-factors, exchange coupling constants, particle sizes, etc., induced by the insertions of Li^+ ions.[21] It is notable that the in-situ magnetic measurements revealed the reduction site change from the A to the B site at 1.8 V, which could not detected by the X-ray diffraction and absorption studies.

The temperature dependence of the magnetizations at the battery voltages of 1.0, 0.5, 0.3, 0.1 and 0 V are shown in Fig. 5(b). The inset of this figure shows the low-temperature behavior on an enlarged scale. Below 1.3 V, the magnetizations exhibit an irreversible change due to a structural change from the inverse spinel to the rocksalt structure, followed by the reduction to Fe metal. The temperature dependence of the magnetizations at 1.0 V, where the PXRD suggests the formation of $Li_xFe_3O_4$, makes a broad maximum around 100 K, which is similar to the magnetic behavior at 0.5 V (see the inset of Fig. 5(b)). Figure S3(a) shows the field-cooled (FC) and zero-field-cooled (ZFC) magnetizations at 1.0 V, which clearly show a bifurcation point at 150 K. This behavior is consistent with the ferrimagnetic order of the rocksalt-type $Li_xFe_3O_4$ at this temperature, as reported previously.[21] As the voltage decreases to 0.3 V, the temperature dependence of the magnetization makes two maxima around 40 and 100 K, which are assignable to Fe nanoparticles and the rocksalt-type $Li_xFe_3O_4$, respectively. With a decrease in the battery voltage down to 0 V, the magnetization maximum around 40 K due to Fe nanoparticles increases significantly. Figures S3(b) and S4 show the FC-ZFC and MH curves for the cathode sample at 0 V, showing a bifurcation point at 40 K and a coercive force, H_c, of 400 Oe at 4 K, respectively. These results can be understood in terms of the superparamagnetic behavior of α-Fe nanoparticles with a diameter of *ca.* 5 nm.[26] This electrochemical milling behavior[32, 33] indicates that SSE would be available for the preparation of nanoparticles of various metal and metal oxides.

It was reported that the Li^+ insertion into Fe_3O_4 immediately induced a local structural change from the inverse-spinel to the rocksalt structure, which was caused by a displacement of Fe^{III} ions from the tetrahedral A site to the octahedral B' site, and then brought about the reduction of Fe^{III} ions at the octahedral sites.[20] This work was done for the Fe_3O_4 particles with a size of *ca.* 50 μm. However, the present research on the valence, structure and magnetic properties of the 30 nm Fe_3O_4 particles, concluded that the Li^+ insertion/Fe^{III} reduction took place in the original inverse-spinel structure in the battery voltage range above 1.3 V. This discrepancy is perhaps caused by the huge difference in the particle size of Fe_3O_4; the nanoparticles of γ-Fe_2O_3 are known to be reduced by the Li^+ insertions in its original structure.[34]

SSE-control magnetizations

Fe_3O_4 was found to exhibit the reversible redox change in the inverse spinel structure, under the electrochemical Li^+ doping in the battery voltage above 1.3 V. To reveal the reversible magnetic response to this redox process, we examined the magnetic properties of Fe_3O_4 controlled by SSE. The Li-Fe_3O_4 battery was inserted into a SQUID susceptometer and its voltage was controlled at room temperature by charging/discharging with a constant current density of 0.03 $mA \cdot cm^{-2}$, in the range between 1.3 and 1.8 V. Then, we carried out the in-situ magnetic measurements at 1 kOe. The results are

shown in Fig. 7, including the observation of a reversible and repeatable change in magnetization of *ca*. 13%. Since the reversible redox change takes place only in the inverse spinel structure, and the conversion to the rocksalt-type $Li_xFe_3O_4$ with T_N of 150 K is irreversible, we could not achieve a more drastic change in magnetism. Even so, the present study strongly suggests the potential development of "electrochemical magnets," in which SSE could induce permanent magnetization at room temperature, thereby avoiding the requirement of a continuously loaded current in order to maintain the magnetization of electromagnets.

Conclusions

We produced Li-Fe_3O_4 batteries in order to carry out in-situ magnetic measurements and ex-situ X-ray structural and absorption analyses of Fe_3O_4 nanoparticles under their solid-state electrochemical reduction to Fe metal. The comprehensive analysis revealed a rechargeable feature of this battery above the voltage of 1.3 V, with a high capacity of 160 A h kg^{-1}, in the original inverse spinel structure of Fe_3O_4. In the range between 1.3 and 1.0 V, magnetite was irreversibly converted to $Li_xFe_3O_4$ with a rocksalt structure due to its more than 1.4-electron reduction. In the battery-voltage range between 0.5 and 0 V, $Li_xFe_3O_4$ was reduced to α-Fe, whose diameter was 5 nm. This reaction was accompanied by the generation of Li_2O. The in-situ magnetic measurements provided information on the redox/spin states of the chemical species, which appeared in the reduction process of Fe_3O_4. Utilizing the electrochemical reversibility of Fe_3O_4 above 1.3 V, we also demonstrated a reversible change in its magnetization at room temperature, which was controlled by SSE. Together, our findings indicated that the in-situ magnetic measurements for SSE are a powerful technique to elucidate the solid-state redox processes and have the potential to lead to new magnetic functions, such as electrochemical magnets.

Acknowledgements

This work was performed with the approval of the Aichi Synchrotron Radiation Center. We thank Dr. H. Asakura and Prof. M. Tabuchi (Nagoya University) for their tremendous help with the XAFS measurements. We are grateful to the Ministry of Education, Culture, Sports, Science and Technology (MEXT) of Japan for a Grant-in-Aid for Scientific Research. This work was also supported by the JSPS Core-to-Core Program, A. Advanced Research Networks.

Notes and references

[a] Research Center for Materials Science & Department of Chemistry, Nagoya University, Furo-cho, Nagoya 464-8602, Japan. E-mail: yoshikawah@chem.nagoya-u.ac.jp, awaga@mbox.chem.nagoya-u.ac.jp; Fax: +81 52 789 2484; Tel: +81 52 789 2487

[b] Core Research for Evolutional Science and Technology (CREST), Furo-cho, Nagoya 464-8602, Japan

† Electronic Supplementary Information (ESI) available: Calculation of battery capacity, an image of in-situ magnetic measurement system, magnetic property of authentic Fe_3O_4 nanoparticles and those at electrochemical process. See DOI: 10.1039/b000000x/

1 B. O'Regan and M. Grätzel, *Nature*, 1991, **353**, 737-740.
2 D. Braga, N. C. Erickson, M. J. Renn, R. J. Holmes and C. D. Frisbie, *Adv. Mater.*, 2012, **22**, 1623-1631.
3 K. Ueno, S. Nakamura, H. Shimotani, H. T. Yuan, N. Kimura, T. Nojima, H. Aoki, Y. Iwasa and M. Kawasaki, *Nat. Nanotechnol.*, 2011, **6**, 408-412.
4 H. Yoshikawa, C. Kazama, K. Awaga, M. Satoh and J. Wada, *Chem. Commun.*, 2007, 3169-3170.
5 H.Wang, S. Hamanaka, T. Yokoyama, H. Yoshikawa and K. Awaga, *Chem. Asian J.*, 2011, **6**, 1074-1079.
6 H. Yoshikawa, S. Hamanaka, Y. Miyoshi, Y. Kondo, S. Shigematsu, N. Akutagawa, M. Sato, T. Yokoyama and K. Awaga, *Inorg. Chem.*, 2009, **48**, 9057-9059.
7 H. Wang, Z. Zeng, N. Kawasaki, H. Eckert, H. Yoshikawa and K. Awaga, *Chem. Eur. J.*, 2013, **19**, 11235-11240.
8 H. Wang, S. Hamanaka, Y. Nishimoto, S. Irle, T. Yokoyama, H. Yoshikawa and K. Awaga, *J. Am. Chem. Soc.*, 2012, **134**, 4918-4924.
9 N. Kawasaki, H. Wang, R. Nakanishi, S. Hamanaka, R. Kitaura, H. Shinohara, T. Yokoyama, H. Yoshikawa and K. Awaga, *Angew. Chem. Int. Ed.,* 2011, **50**, 3471-3474.
10 H. Wang, N. Kawasaki, T. Yokoyama, H. Yoshikawa and K. Awaga, *Dalton Trans.*, 2012, **41**, 9863-9866.
11 T. Yamada, K. Morita, H. Wang, K. Kume, H. Yoshikawa and K. Awaga, *Angew. Chem. Int. Ed.,* 2013, **52**, 6238-6241.
12 N. Amin and S. Arajs, *phys. stat. sol. (a)*, 1986, **97**, 479-484.
13 Z. Z. Zhang, S. Cardoso, P. P. Freitas, X. Batlle, P. Wei, N. Barradas and J. C. Soares, *J. Appl. Phys.*, 2001, **89**, 6665-6667.
14 J. W. M. Bulte and D. L. Kraitchman1, *NMR Biomed.*, 2004, **17**, 484-499.
15 M. Ma, Y. Wu, J. Zhou, Y. Sun, Y. Zhang and N. Gu, *J. Magn. Magn. Mater.*, 2004, **268**, 33-39.
16 E. J. Verwey, P. W. Haayman and F. C. Romeijn, *J. Chem. Phys.*, 1947, **15**, 181-187.
17 Z. Janu, J. Hadac and Z. Svindrych, *J. Magn. Magn. Mater.*, 2007, **310**, e203-e205.
18 H. Deng, X. Li, Q. Peng, X. Wang, J. Chen and Y. Li, *Angew. Chem. Int. Ed.*, 2005, **44**, 2782-2785.
19 S. K. Behera, *J. Power Sources,* 2011, **196**, 8669-8674.
20 M. M. Thackeray, W. I. F. David and J. B. Goodenough, *Mat. Res. Bull.*, 1982, **17**, 785-793.
21 J. Fontcuberta, J. Rodríguez, M. Pernet, G. Longworth and J. B. Goodenough, *J. Appl. Phys.*, 1986, **59**, 1918-1926.
22 V. Sivakumar, S. Kumar, C. A. Ross and Y. S. Horn, *IEEE Trans. Magn.*, 2007, **43**, 3121-3123.
23 J. M. Neto, E. Nunez and P. H. Domingues, *J. Mater. Sci. Lett.*, 1997, **16**, 231-233.
24 M. B. Pinson and M. Z. Bazant, *J. Electrochem. Soc.*, 2013, **160**, A243-A250.
25 G. N. Glavee, K. J. Klabunde, C. M. Sorensen and G. C. Hadjipanayis, *Inorg. Chem.*, 1995, **34**, 28-35.
26 D. L. Huber, *Small*, 2005, **1**, 482-501.

27 M. C. Menard, K. J. Takeuchi, A. C. Marschilok and E. S. Takeuchi, *Phys. Chem. Chem. Phys.,* 2013, **15**, 18539-18548.
28 Q. Liu, Y. Yan, X. Yang, J. Qian, J. Cai and K. Wang, *J. Electroanal. Chem*., 2013, **704**, 86-89.
29 A. L. Patterson, *Phys. Rev*., 1939, **56**, 978-982.
30 G. F. Goya, T. S. Berquó, F. C. Fonseca, and M. P. Morales. *J. Appl. Phys*., 2003, **94**, 3520.
31 L. Gao, R. Li, and Q. Chen, *J. Phys. D: Appl. Phys.*, 2012, **45**, 335001.
32 Y. Hu, Y. Guo, W. Sigle, S. Hore, P. Balaya and J. Maier, *Nat. Mater*., 2006, **5**, 713-717.
33 D. Zhang, C. Chen, J. Zhang, and F. Ren, *Chem. Mater*., 2005, **17**, 5242-5245.
34 S. Kanzaki, T. Inada, T. Matsumura, N. Sonoyama, A. Yamada, M. Takano, R. Kanno, *J. Power Sources*, 2005, **146**, 323.

Table of contents entry

Comprehensive study on the solid-state electrochemical reduction process of magnetite (Fe_3O_4) nanoparticles in Li batteries, reveals a rechargeable battery performance and a controllable change in magnetization.